

Switched Tank Converters

Shuai Jiang*, Stefano Saggini†, Chenhao Nan*, Xin Li*, Chee Chung*, Mobashar Yazdani*

*Google Inc.

1220 N. Mathilda Ave, Sunnyvale, CA 94089

†DPIA - University of Udine

Via delle Scienze 208, 33100 Udine, Italy

Email: shuaij@google.com, stefano.saggini@uniud.it, chenhao@google.com, xinxli@google.com, cheec@google.com, myazdani@google.com,

Abstract—This paper presents a new class of Switched Tank Converters (abbreviated as STCs) for high efficiency high density non-isolated DC-DC applications where large voltage step down (up) ratios are required. Distinguished from switched capacitor converters, the STCs uniquely employ LC resonant tanks to partially replace the flying capacitors for energy transfer. Full soft charging, soft switching and minimal device voltage stresses are achieved under all operating conditions. The STCs feature very high efficiency, power density and robustness against component non-idealities over a wide range of operating conditions. Furthermore, thanks to the full resonant operation, multiple STCs can operate in parallel with inherent droop current sharing, offering the best scalability and control simplicity. These attributes make STC a disruptive and robust technology viable for industry's high volume adoption. A novel equivalent DCX building block principle is introduced to simplify the analysis of STC. A 98.9% efficiency STC product evaluation board (4-to-1, 650W) has been developed and demonstrated for the next-generation of 48V bus conversion for data center servers.

Index Terms—Switched tank converters, switched capacitor converters, soft charging, soft switching, DCX.

I. INTRODUCTION

Recent advancement of semiconductor power devices including both wide-band-gap devices (GaN and SiC) and silicon devices (Trench MOS, LDMOS, etc.) has been pushing power conversion to higher efficiency and density, due to the continuous improvement of the device Figure of Merits (FOM). In the meantime, however, passive components including capacitors and magnetics do not obey Moores law. Particularly in many modern power electronics applications, magnetic components are becoming bottlenecks in terms of further efficiency and density improvement. For instance, in telecom and data center motherboards where high ratio DC-DC bus conversion is often required, transformer based topologies such as active-clamp forward, full bridge and LLC resonant converters are prevailing regardless of galvanic isolation requirement. Transformer design and integration for these topologies have become the greatest challenge for system optimization as it heavily dictates the overall system efficiency and density. On the other side, the huge customization effort associated with transformers has been hindering some critical business considerations such as scalability, cost, manufacturing risks, and time to market as well [1].

Switched capacitor converters (SCCs) have been widely investigated in both academia and industry for many years, covering a variety of applications from mW level to kW level, from point-of-load PMICs to electrical vehicle power systems [2]- [15]. Instead of using bulky magnetics to achieve voltage step down (up), SCCs primarily rely on switches and capacitors to do the similar job by stacking voltages. The inherent nature of high density and magnetic-less with SCCs becomes compelling from the system design perspective. However, a critical fundamental limit of SCCs is well known as the charge redistribution loss mechanism [16]. Whenever a low-impedance switch is closed between two capacitors, the voltage mismatch between capacitors leads to a current inrush and charge redistribution [17]. To minimize the energy loss associated with this charge redistribution, larger capacitors and higher switching frequency are usually required than what they are ideally wanted to be. Hence, either power density or efficiency needs to be sacrificed which offsets the benefit of being magnetic-less.

To address the charge redistribution loss problem of traditional SCCs, many derivative architectures have been proposed and investigated [18]- [22]. The key concept is to introduce some inductive elements into the SCCs such that the charging and discharging of the SCC flying capacitors are essentially lossless. Depending upon the specific topology and PWM control approach, one can achieve soft charging (current-source-like inductive charging) [20], [22], [23] or soft switching (ZVS/ZCS) or both. A merged two-stage SCC-buck architecture incorporating the soft-charging concept was first presented in 2008 [18]. Later on, a start-up company named Arctic Sand was founded based on this architectural concept. It offers high efficiency high integration backlight LED drivers and point-of-load voltage regulators for mobile applications. In brief, this merged two-stage architecture elegantly couples the buck inductor to the first SCC stage to softly charge and discharge the flying capacitors. Even though this merged two-stage approach is promising for end-to-end conversion, it is less convenient in applications where independent general-purpose bus converters are more desirable. Another solution to achieve soft charging is to incorporate inductors in the SCC itself. Multiple approaches have been reported in the existing literatures. First, certain number of inductors are aggregated

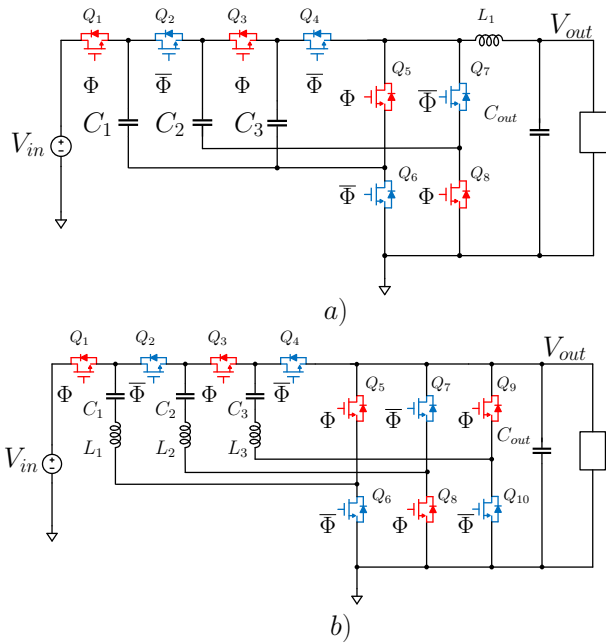


Fig. 1: Examples of prior SCC derivative topologies with inductors. (a) 4-to-1 Dickson SCC with one aggregated inductor; (b) 4-to-1 Multi-level Modular SCC with distributed inductors.

at specific circuit nodes of an SCC topology regardless of the switch and capacitor count [24]- [28]. Each of the inductors can be coupled to multiple flying capacitor networks during each switching state. The inductor current can be either a pure AC or a DC plus some AC ripples, depending upon the specific inductor locations in the circuit. One example of SCC using an aggregated inductor is given in Fig. 1(a). Second, inductors can be distributed in an SCC topology as well [21], [29], [30]. The inductor count increases along with switch and capacitor count. In certain circumstances, stray inductors can be used. One example of SCC with distributed inductors is shown in Fig. 1(b). Regardless of using aggregated inductors or distributed inductors in SCCs, multiple ways of PWM control are available to achieve not only soft charging but also resonant soft switching (ZVS [31]- [34] or ZCS [21], [24]- [27], [29], [30], [35]- [37]) and regulation [38], [39].

From the above-mentioned, it seems plenty of SCC derivative solutions are available and ready for the industry to adopt for wide and high volume use. However, in order to make any of these SCC based solutions viable for mass production design, a lot more hidden challenges behind the scene are something that the industry can't get around and must be addressed. In this paper will be discussed a new class of switched capacitor based converters defined as Switched Tank Converters (abbreviated as STCs and first introduced in [1]) in order to overcome some limitation to the wide use of such kind of solutions. The paper is organized as follows. In the next section will be described the main problems related to the usage of SCC converter as component non-idealities, stress and scalability. After considering all these practical challenges discussed above, a disruptive new class of Switched Tank Con-

verters (STCs) are proposed in Section III. The key attributes of STCs will be elaborated. An equivalent DCX building block modeling approach is then introduced in Section IV for STC circuit analysis. By using this model the analysis of mismatch effects are analyzed in section V. One STC topology has been selected for the 48V data center bus converter application described in section VI. A fully functional 650W 4-to-1 STC product evaluation board has been developed. Experimental performance data will be demonstrated in Section VII and the conclusion will be drawn in Section VIII.

II. SCC APPLICATION CHALLENGES

In this section will be discussed the main obstacles to the uses of SCC solution in widespread applications considering high volume robustness, reliability and the device technology opportunity in the market. The immunity to component variations and parasitics, voltage stress of MOSFETs and issue related to the scalability of these solutions will be covered.

A. Immunity to component non-idealities

Most of the above-mentioned topologies are using Class II ceramic capacitors (X7R, X7S, X5R, etc.), which inherently have a very wide tolerance band over temperature (e.g., up to $\pm 22\%$ for X7S), DC bias (e.g., a 100V Class II MLCC can derate by 70% with 50V bias) and part-to-part variation (higher than $\pm 10\%$). However, these topologies often rely on precisely determined flying capacitors to either satisfy full soft charging requirement [22] or match the switching frequency to LC resonance for soft switching. In addition, the parasitic loop inductances can't be ignored in high current applications. Therefore, the electrical characteristics consistency among different products can hardly be guaranteed once the volume goes high. Undesirable corner cases tend to show up from Monte Carlo or worst case analysis. In some other cases, topologies with distributed inductors, for instance, the one shown in Fig. 1(b), create a lot of challenges to designing for all possible inductor current commutation paths during dead time considering LC tolerances and control timing mismatches. A converter topology whose electrical characteristics vary heavily with component mismatches, large tolerances, or loop parasitics is not viable for industry production.

B. Capacitor material consideration

In most SCC topologies, the electrical characteristics (operation modes, current waveforms, output impedance, losses, etc.) are often associated with flying capacitor values. While Class II ceramic capacitors with large variations are mostly seen in existing literatures, Class I ceramic capacitors are rarely evaluated and used in SCC topologies. Class I ceramic capacitors (COG, U2J, etc.) use very low dielectric constant and low loss factor dielectric material to offer very stable capacitance, low tolerance (less than $\pm 5\%$) and low ESRs across all operating conditions. They are ideal capacitor candidates for SCCs that require tight capacitor matching, resonant operation and high current. However, due to the very low dielectric constant and small capacitance, Class I ceramic capacitors usually

carry much higher AC voltage ripples than Class II ceramic capacitors in power conversion. It becomes undesirable if switching MOSFETs can see these ripples across drain to source. Therefore, how to appropriately apply Class I ceramic capacitors to SCC based topologies and fully leverage their superior electrical performance remains a challenge.

C. Worst case voltage stress of MOSFETs

One of the key enablers for high efficiency high density of SCC based topologies is the opportunity to use low voltage rating MOSFETs with better FOMs. For example, in a step-down Dickson and its derivative SCC topologies, all switching devices have either V_{out} or $2V_{out}$ as maximum drain source voltage during normal operation regardless of the high side V_{in} . However, in order to reliably use low voltage devices, the voltage stress of these devices should never exceed their absolute max rating under all worst case circumstances. The simplest question to ask is whether the drain-to-source voltage of each device can always be clamped to a minimal DC-like voltage by a capacitor or capacitor network in the OFF state even considering loop parasitic inductances, transient events, and worst case component variations. Apparently, the FETs (Q1-Q4) in Fig. 1(b) are not desirably clamped and thus can go over stress easily during switching transitions.

D. Scalability

In high current applications, there are two main aspects that must be considered for scalability: 1) the scalability of the topology itself to different conversion ratios and power ratings; 2) the scalability of the control/driver circuitry. For the first part, it's needed to examine how the circuit electrical characteristics change according to different conversion ratios, how easy to accommodate those changes, whether multiple converters can be connected in parallel with good current sharing, and so on. For the second part, it is desirable to have a simple uniform central controller and a scalable driver circuit that supports all topology configurations. In some cases, additional voltage sensing across floating flying capacitors are required to achieve 100% soft charging [28]. This type of complication also affects the scalability of control.

E. Minimum RMS current

In applications where conduction losses are often dominant at heavy load, minimizing RMS current of each component becomes critical. In order to achieve this goal, it is ideal to control an SCC based topology with or close to two symmetric switching states at near 50% duty cycle. And in each switching state, current waveform should be definitive with least influence from parasitic ripples due to component non-idealities. Hence, current can be evenly delivered with minimum RMS. In some resonant SCC topologies using aggregated inductors, the same inductor may resonate with different capacitor banks in different switching states such that asymmetric duty cycle must be used to accommodate multiple resonant frequencies. In these cases, RMS current is not minimized.

F. Thermal performance

It is always desirable to have even temperature distribution within the converter without having hot spots. This allows the converter to be capable of delivering maximum power under a given thermal environment. In other words, a good SCC topology needs to have the power stresses distributed among the devices as evenly as possible. By carefully considering all these practical challenges discussed above, a disruptive new class of Switched Tank Converters are proposed in the following sections.

III. SWITCHED TANK CONVERTER TOPOLOGIES

In this section the key attributes of STC topologies will be defined. Similar to the examples reported previously in Fig. 1, STCs adopt magnetic components to perform ZCS and soft switching operation but overcoming the limitations treated in the previous section. This class of topologies can be derived from SCC structures with two topological states. The transformation of an SCC to an STC topology or the creation of a new architecture is based on composition of elementary cells. Each cell can be defined as a building block that can have two different basic structures reported in Fig. 2(a) and (b). Obviously, neither of these two building blocks can work alone. They both need an additional common mode current path between input and output in order to function correctly. For example, IN_- can be tied to a DC source while OUT_- is tied to reference ground. In Fig. 2 is reported a voltage generator V_{cm} with a given impedance Z_{cm} that represents the different voltage level between input and output terminals. In this condition two STC building blocks operate on the DC values as 1:1 ideal DC transformer (DCX). The DC filtering capacitor C_F and the resonant capacitor C_R can both block the common-mode voltage difference between input and output. A detailed model on the average values of the input current and input voltage will be addressed in the next section. The STC architecture is obtained by connecting the input and/or the output port of the buildings blocks in serial or/and in parallel. The resonant block of Fig. 2(a) pairs with the block of Fig. 2(b) to essentially form a resonant operation in which the resonant building block generates a resonant current by switching approximately at the resonant frequency. The non-resonant building block stabilizes the voltage of the input and output terminals by connecting C_F (with $C_F \gg C_R$) to ground or to another stable voltage. *Substantially each combination of building blocks in which the devices during the ON time conduct one half period of resonant current and during the OFF time have a voltage drop defined by a mesh of DC filtering capacitors as C_F and/or capacitors connected to ground can be defined as an STC.* The simplest STC structure realizable is a 2-to-1 resonant SCC that requires only the building block of Fig. 2(b) with the input port (IN_+ , IN_-) and the output port (OUT_+ , OUT_-) connected in series. The input voltage V_{in} is across the series and the output voltage V_{out} is connected on the output port of the building block. Some examples of STC topology construction developed from an SCC are reported in Fig. 3 and in Fig. 4. The two topologies are derived from a Dickson SCC converter

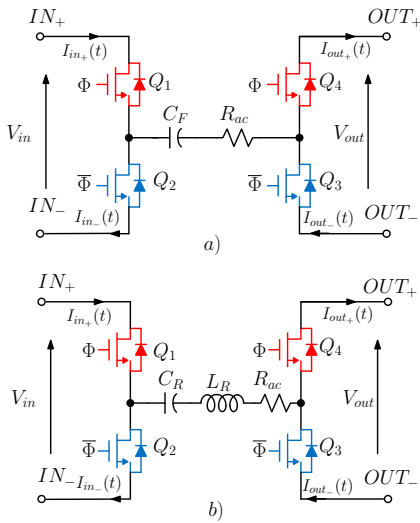


Fig. 2: Two fundamental building blocks of an STC topology: (a) structure with a clamping capacitor; (b) structure with a resonant tank.

and can be considered an extension of the 2-to-1 structure. In fact, by using the building block approach, the topology can be easily considered a serial connection of the input ports of the building blocks from V_{in} to V_{out} and a parallel connection of the output ports from ground to V_{out} , as reported in Fig. 3(a). The choice of composing two resonant blocks and one with the clamping capacitor is to maintain a resonant current in all the branches and to clamp the device off voltage. After it is possible to simplify the redundant switches and obtain the structure of Fig. 3(b). Note that the key features of this architecture is based on the alternation of the two different cells that ensures the ZCS in all the switches and a stable off voltage over the presence of parasitic components. In fact the structure reported in Fig. 1(b) can be described by the connection only of resonant building blocks and cannot be defined as an STC converter. The building block of Fig. 2(a) have the main scope of maintaining the stable off voltages of the devices over the oscillation due to the loop inductors present on the layout. Another solution based only on the resonant building block is reported in Fig. 4. In this case the voltage of the input terminals is clamped by capacitors connected to ground. These clamping capacitors here can be very small as their current ripples are mostly cancelled out. Even if each switch has the off voltage equal to V_{out} this solution requires more switches because merging redundant switches cannot take place. In this way the issues regarding the voltage stress of devices reported in the previous section are not present.

In terms of the current flow direction in the switches, all the switches can be divided into two categories: main switches and synchronous-rectifier (SR) switches. Taking N-Channel MOSFET as an example, a main switch has its current flow from drain to source in normal operations, vice versa, an SR switch normally has its current flow from source to drain. In certain applications, SR switches can be replaced by schottky diodes. In a step-down STC, all the switches are normally

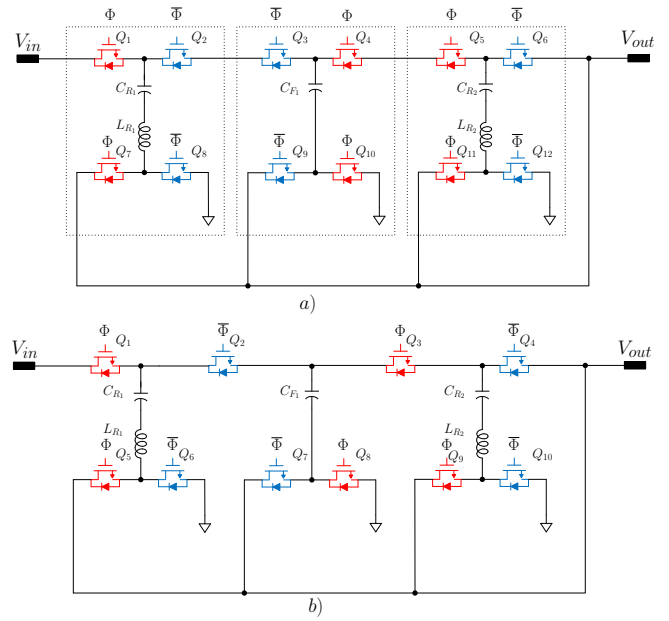


Fig. 3: 4-to-1 STC derivation: (a) structure with building blocks; (b) 4-to-1 STC topology derived.

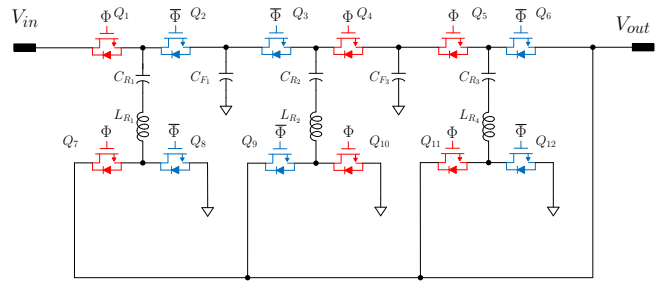


Fig. 4: 4-to-1 STC (1-phase, all switches clamped by V_{out}).

blocking either V_{out} or $2V_{out}$ in their OFF state. Therefore, low voltage devices with superior FOMs can be used to switch faster and achieve smaller conduction loss, which is the key enabler for both high efficiency and high density. It is often a good practice to design the topology with evenly shared current stresses so that temperature becomes equally distributed, and circuit layout becomes more convenient. The flying capacitors in STCs are characterized by two categories: resonant capacitors C_R and DC filtering capacitors C_F . Each resonant capacitor is in series connection with a resonant inductor to essentially form an LC resonant tank. Multiple LC tanks that share the same resonant frequency are incorporated in an STC to partially replace the original DC flying capacitors in SCCs. Therefore, instead of switching and transferring energy between flying capacitors like traditional SCCs, in an STC, the energy is always being transferred between one LC tank and another LC tank or a DC filtering capacitor during switching. This characteristic explains the topology name Switched Tank Converters. Different types of technologies are adopted for the two categories of capacitors in order to overcome the limitation reported in the previous section. High performance Class-I (e.g., C0G, U2J) MLCC capacitors can be used as resonant capacitors in an STC. Their tight

tolerance ($\pm 5\%$) and low ESR (dissipation factor 0.1%) over a wide voltage and temperature range are perfectly suitable for resonant operation. Class-II (e.g., X7R, X6S, etc.) MLCC capacitors that offer much higher capacitance than Class-I capacitors are used as DC filtering capacitors, which serve for the DC filtering and clamping functions. Because a DC filtering capacitor works almost like a DC voltage source with very minimal AC ripples, it has negligible impact to the resonant operation of STC. This makes the STC operation very insensitive to the large tolerances of the Class-II MLCC capacitors. Benefiting from the resonant operation of the LC tanks, all the switches in an STC can be controlled to turn on and off upon current reaching zero. This zero current switching (ZCS) feature allows an STC to be almost free of switching losses, particularly in low voltage applications where MOSFET C_{oss} charge losses are much less significant. Hence, an STC can inherently achieve very high efficiency. As the resonant capacitors are Class-I ceramics with $\pm 5\%$ tolerance, using matched resonant inductors to get a uniform resonant frequency across all the LC tanks becomes viable. As will be detailed in Section V, in order to tolerate more tank-to-tank variations, simple zero current detection (ZCD) techniques can be applied as well to adaptively control the ON time for each resonant tank such that each LC resonant frequency is always in track. One of the most critical features of an STC is that every individual current conduction sub-circuit loop sees at least one LC resonant tank with inductive impedance at high frequency. Therefore, every flying capacitor is always being softly charged and discharged during operation. This key characteristic fundamentally eliminates the previously mentioned inrush current or charge redistribution losses associated with traditional SCCs. Compared to the previously mentioned topologies that incorporate aggregated inductors for soft charging, the soft charging of STC is 100% guaranteed regardless of flying capacitor matchings and tolerances.

In order to reliably leverage the superior FOMs of low voltage rating MOSFETs, all switch drain-to-source voltages must be always clamped to desired DC levels by DC capacitors or capacitor networks. The DC filtering flying capacitors in STC naturally serve for this purpose. Even though multiple inductors are employed in an STC, none of the switches will see them in series at the OFF state. Instead, at any switching state, all the off switches are always clamped at either V_{OUT} or $2V_{OUT}$ by the DC flying capacitors and input/output capacitors. This ensures the reliable use of low voltage rating devices with minimal voltage stresses.

Enabled by the definitive output impedance, same STCs can be connected in parallel to operate in multi-phase or multi-cell manners. The PWM clocks among paralleled phases or cells can be synchronized with or without phase interleaving, or even non-synchronized. Inherent droop current balancing among phases or cells is achieved by using the same MOSFETs and LC tanks. This feature provides a great scalability of STCs to higher current and higher power. From the previously discussed, Table I here summarizes the comparisons of the most critical attributes of STCs and existing SCC topologies.

Fig. 4 shows a 1-phase 4-to-1 STC with all switches

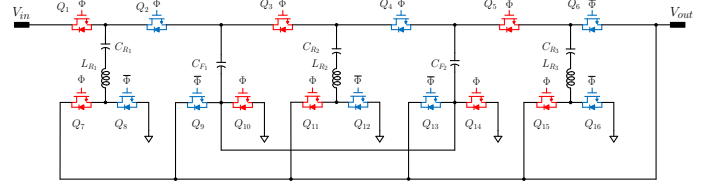


Fig. 5: 6-to-1 STC (1-phase, all switches clamped by V_{out} and $2V_{out}$).

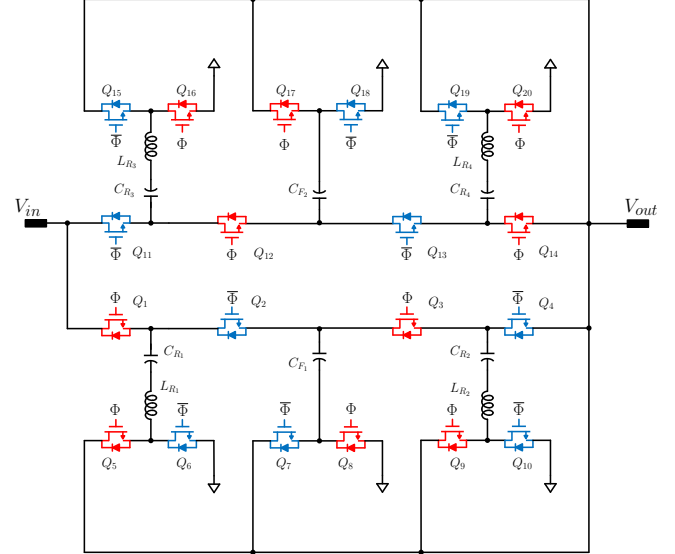


Fig. 6: 4-to-1 STC (2-phase, all switches clamped by V_{out} and $2V_{out}$).

clamped by V_{out} . Q_1-Q_6 are the main switches, Q_7-Q_{12} are the SR switches. There are three LC resonant tanks (branch with L_R and C_R) and two DC filtering capacitors C_F with much lower voltage ripples (cancelled out) than the resonant capacitors C_R . In this topology, the C_F capacitors are biased by different DC voltages ($2V_{out}$ and $3V_{out}$) during normal operation. A 1-phase 4-to-1 STC with all switches clamped by V_{out} and $2V_{out}$ is shown Fig. 3(b). In this topology, Q_2-Q_3 and Q_4-Q_5 are merged to a single switch with double voltage rating, respectively. DC filtering capacitors and resonant tanks are re-arranged. Fig. 5 shows a 1-phase 6-to-1 STC which is scaled up from Fig. 3(b). C_{F1} and C_{F2} are connected together at one side here to provide a shorter clamping loop for Q_3 and Q_4 . In Fig. 3(b) and Fig. 5, Class II ceramic capacitors are selected for C_F . This allows the resonant frequency to be determined pretty much only by L_R and C_R with very tight tolerance. Because the topology of Fig. 3(b) and Fig. 5 uses less switches and passive components, this topology becomes very compelling particularly in low voltage (e.g., 48V) high current applications. The conversion ratio of this topology can be conveniently scaled up and down to even integers. As discussed earlier, STCs can support parallel operation for higher power by using multi-phase or multi-cell configurations. Fig. 6 shows the 2-phase 4-to-1 STC topology derived from Fig. 3. 180 deg phase interleaving allows to minimize input current ripple and decoupling capacitors.

TABLE I: comparison between SCC and STC topologies

	SCCs	SCCs with aggregated inductors [24]-[28]	SCCs with distributed inductors [21], [29] and [30]	STCs
Soft charging	No	Partial	Full	Full
Soft switching capability	No	Yes	Yes	Yes
Immunity to component non-idealities	Poor	Medium	Very poor	Very good
Device voltage clamp	Clamped, low stress	Case by case	No clamp, very high stress	Clamped, low stress
Scalability	Poor	Medium	Very good	Very good

IV. ANALYSIS OF THE STC TOPOLOGIES

A. STC modeling

In this section the state space average (SSA) circuit of a building block is introduced to make the circuit analysis of STC very simple and intuitive based on the approach described in [17], and in [41]–[43]. Each building block of Fig. 2(a) and (b) are driven by two gate signals, reported in Fig. 8(a), G_ϕ and $G_{\bar{\phi}}$ that are active during ϕ and $\bar{\phi}$ phase respectively with a dead time T_d . Each building block can be substituted by the block of Fig. 7 composed by a DC transformer and an equivalent impedance expressed as Z_{eq} . The impedances Z_{io} carry the current induced by the common mode voltage difference between the input and output port terminals. It can be easily concluded that this impedance can be approximated to

$$Z_{io} \approx \frac{2}{sC_{eq}} \quad (1)$$

where C_{eq} is C_F and C_R respectively for the building block of Fig. 2(a) and (b). The inductance L_R doesn't play a role because the resonant frequency is equal to the switching frequency and the SSA model is applicable for lower frequency. Based on the equivalent model in Fig. 7, it can be simply proven that as long as the DC blocking voltage of the transformer remains constant with dynamic load, the common mode impedance Z_{io} can be neglected. In an STC topology, the DC bias voltage of each flying capacitor represents the DC blocking voltage of the equivalent transformer in Fig. 7, and it will remain approximately constant under dynamic load assuming the resonant tank building blocks are approximately matched. Apparently, any input line voltage dynamics will generate common mode current through Z_{io} impedances. However, the line voltage dynamics are often much slower than load dynamics in many applications, such that the contribution of Z_{io} impedances can be neglected as well. For the sake of simplicity the calculation of the Z_{eq} is applied first on an ideal (high Q, $R_{ac} \approx 0$) resonant building block. In order to calculate this contribution the circuit of Fig. 2(b) will be analyzed with a fixed input voltage V_{in} and output voltage V_{out} . This resonant switching circuit with a negligible R_{ac} is excited by V_{in} higher than V_{out} and the terminals IN_- and OUT_- are connected to ground. It exhibits the behavior reported in Fig. 8(a) in which are reported the voltage across the resonant tank V_{TR} , the voltage across the capacitor V_{C_R} and the current I_{L_R} . Each switch is turned on

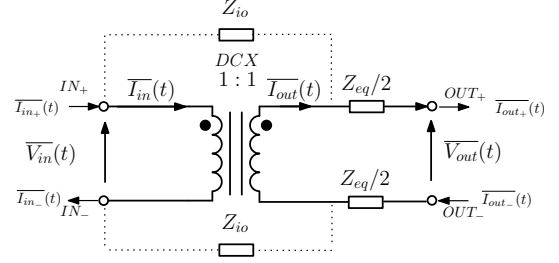


Fig. 7: Equivalent SSA model for a building block.

for a period equal to $T_R/2$ and a dead time T_d is present before the turn on of the complementary one. In this electrical condition the $I_{L_R}(t)$ exhibits a sinusoidal transient behavior positive or negative with an amplitude \hat{I}_{L_Rk} that satisfies the relation (2) based on the conservation of the energy.

$$\frac{\hat{I}_{L_Rk}^2 L_R}{2} - \frac{\hat{V}_{C_{Rk-1}}^2 C_R}{2} = (V_{in} - V_{out}) \frac{\hat{I}_{L_Rk} T_R}{2\pi} \quad (2)$$

Considering a period T_{sw} the conservation of the energy can be expressed in relation of the voltage $\hat{V}_{C_{Rk}}$:

$$\frac{\hat{V}_{C_{Rk}}^2 C_R}{2} - \frac{\hat{V}_{C_{Rk-1}}^2 C_R}{2} = (V_{in} - V_{out}) \frac{\hat{I}_{L_Rk} T_R}{\pi} \quad (3)$$

Subtracting each element of (2) expressed for the $k+1$ period from the same equation expressed for the k period and substituting the energy of the capacitor expressed in (3) we can obtain

$$\frac{\hat{I}_{L_{Rk+1}}^2 L_R}{2} - \frac{\hat{I}_{L_{Rk}}^2 L_R}{2} = (V_{in} - V_{out}) \frac{\hat{I}_{L_{Rk+1}} + \hat{I}_{L_{Rk}}}{2\pi} T_R \quad (4)$$

Note that the same relation can be calculated considering the conservation of the energy in a period between two peaks of the inductor currents. By simplifying (4) it is possible to obtain

$$V_{in} - V_{out} = L_R \frac{\pi}{T_R} \left(\hat{I}_{L_{Rk+1}} - \hat{I}_{L_{Rk}} \right) \quad (5)$$

The variation of the $\overline{I_{out}(t)}$ over a period of T_{sw} can be derived as:

$$V_{in} - V_{out} = \frac{\pi^2 T_{sw}^2}{T_R^2} L_R \frac{\overline{I_{out}(t+T_{sw})} - \overline{I_{out}(t)}}{T_{sw}} \quad (6)$$

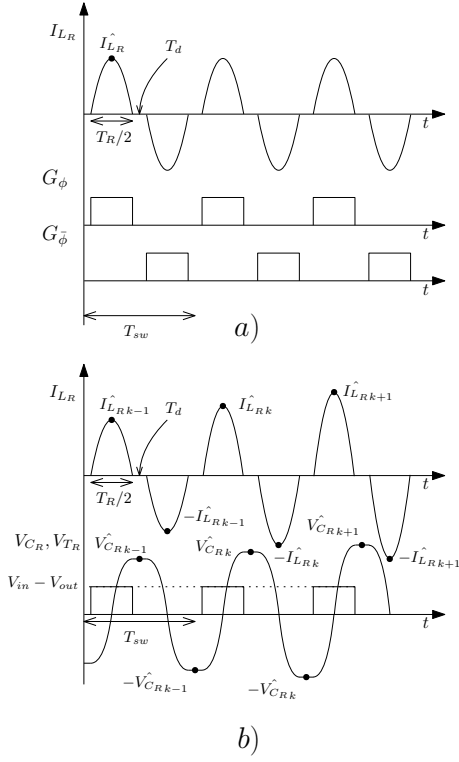


Fig. 8: Driving signals (a) and waveforms (b) of the building block of Fig. 2(b).

From (6) an equivalent inductor that represents the Z_{eq} impedance of Fig. 7 can be derived.

$$L_{eq} = \frac{\pi^2 T_{sw}^2}{T_R^2} L_R \quad (7)$$

Considering the presence of the lumped resistance R_{ac} that contains the R_{dsON} contribution of the switches and all the losses of the resonant tank components, the equivalent resistance can be calculated by equaling the power dissipated by the tank during the operating phases and the power dissipated by the equivalent circuit with the average current $\bar{I}_{out}(t)$. The same approach was followed [17] obtaining a general expression for SCC impedance for soft and hard charging conditions. The equivalent resistance of the building block R_{eq} can be derived considering the case of unity gain switched capacitor cell that operates in soft charging with a high Q resonance.

$$R_{eq} = \frac{\pi^2 T_{sw}}{2T_R} R_{ac} \quad (8)$$

Obviously the equivalent impedance Z_{eq} of the building block of Fig. 2(a) with the clamping capacitor $C_F \gg C_R$ contains only the contribution of R_{eq} .

Taking the STC topology in Fig. 3(b) as an example, Q_2 and Q_3 can be split into two switches as was done for the synthesis in the previous section, reported in Fig. 3(a). The SSA equivalent circuit of the entire converter can be easily obtained by replacing each building block in the dashed box with the corresponding DCX model depicted in Fig. 7. Therefore, the 4-to-1 STC topology SSA model is composed by a matrix configuration of 3 DCX building blocks with

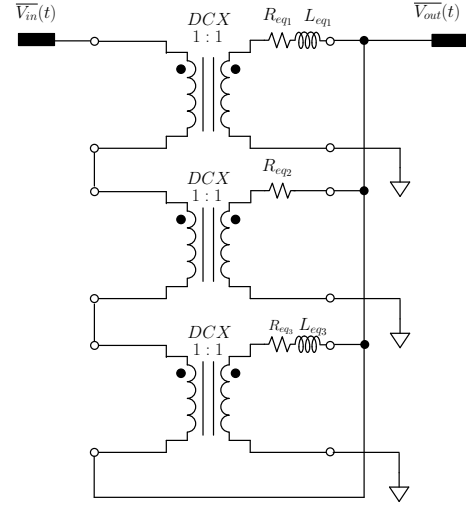


Fig. 9: Equivalent SSA model of the converter reported in Fig. 3(b).

their impedances as shown in Fig. 9. During load transient, or equivalently for the computation of the output impedance, there is negligible variation of the common mode voltage difference between the input terminals and output terminals. Hence in this case Z_{io} can be neglected. While in the line voltage dynamic event, or in the input impedance calculation, common mode current that charges all the flying capacitors and the Z_{io} impedance should be taken into account. In Fig. 9, the DCX input terminals are connected in series and the outputs are connected in parallel. Each DCX block processes 1/4 of the total power. The IN- terminal of the 3rd DCX block is connected to V_{out} such that the last 1/4 power is simply bypassed to the output. Likewise, the other STC topologies can be modeled by the matrix DCX equivalent circuit in the same manner. By simplifying the circuit the total output impedance is

$$R_{eqout} = \sum_{i=1}^{N-1} \frac{R_{eqi}}{N^2} \quad (9)$$

and

$$L_{eqout} = \sum_{i=1}^{N-1} \frac{L_{eqi}}{N^2} \quad (10)$$

where N is equal to 4 and $L_{eq2} = 0$.

By extending the matrix DCX model in Fig. 9 to N -to-1 conversion, the STC output impedance can be again described by (7)-(10). Assuming T_{sw} is sufficiently close to T_R , R_{eqout} is then only determined by R_{ac} of each STC building block. Equation (9) indicates that multiple STCs can operate in parallel with inherent droop current balancing. The R_{ac} mismatch between STCs is reasonably small such that a good current balancing accuracy can be achieved (e.g., 10%).

In Fig. 10 are reported the comparison of transient waveforms from 10A-40A with an input voltage of 54V applied to the circuit of Fig. 3(b) and its equivalent SSA model of Fig. 9. The main system parameters are: $C_R = 3.8\mu F$, $C_F = 60\mu F$, $L_R = 58nH$. The lumped ac resistance is $R_{ac} = 7m\Omega$

for the resonant tank building block and $R_{ac} = 5m\Omega$ for the clamping capacitor building block respectively. Finally the output capacitor is composed of one $470\mu F$ electrolytic capacitor with $ESR = 10m\Omega$ and 20 X6S MLCC capacitors of $22\mu F$ ($7\mu F$ by considering the derating factor due to the DC bias) with $ESR = 3m\Omega$ each. As can be seen there is a good match of the converter dynamics shown in Fig. 10 (a,b). Fig. 10(c) shows the comparison of AC simulations of the output impedance using SIMPLIS. The red line is the result obtained on the actual STC circuit and the blue line represents the associated SSA model. Finally in Fig. 10(d) are reported the voltages V_{CR1} , V_{CR2} and V_{CF} of the flying capacitors during the load transient. It shows that the bias voltage across V_{CF} , V_{CR1} , and V_{CR2} can be considered constant, making the contribution of Z_{io} in the SSA model negligible. Applying the same principle based on the matrix DCX circuit model, many other interesting circuits can be derived potentially. For example, by reconnecting the IN- terminal of the 3rd DCX block in Fig. 9 to a 4-switch buck-boost regulator's input and connecting this buck-boost output in parallel with the STC output, a high efficiency partial power STC-buck-boost topology with voltage regulation capability can be obtained. The DCX building block principle can be used as a simple and effective analytical tool as well to model many other SCC based topologies.

B. Design guidelines

Finally the building block model introduced above is a good design tool to define the components starting from the converter specifications. As described before the STC converter is constructed by a matrix connection of multiple fundamental building blocks that in general process part of the total output power. Each building block can be described by its SSA model characterized by the maximum output mean current, differential voltage across the primary/secondary side and common-mode voltage from primary terminals to secondary terminals (defined as V_{cm} in Fig. 2). All these electrical quantities can be useful to define the maximum voltage and current of the components. The maximum bias voltage of each flying capacitor (including both the resonant capacitor C_R and the DC blocking capacitor C_F) is equal to the common-mode DC blocking voltage from the primary terminals to the secondary terminals of each building block. Considering the maximum output current for a given building block as $\overline{I_{out_m}}$, the maximum peak current \hat{I}_{C_m} and the rms current I_{CRMSm} for each capacitor can be calculated as follows:

$$\hat{I}_{C_m} = \overline{I_{out_m}} \pi \frac{T_{sw}}{T_R} \quad (11)$$

$$I_{CRMSm} = \frac{\hat{I}_{C_m}}{\sqrt{2}} \sqrt{\frac{T_R}{T_{sw}}} \quad (12)$$

As previously mentioned in Section III, high performance Class-I (e.g., C0G, U2J) MLCC capacitors should be used as resonant capacitors C_R , meanwhile Class-II (e.g., X7R, X6S, etc.) MLCC capacitors that offer much higher capacitance are used as DC filtering/clamping capacitors C_F . In both cases,

TABLE II: Switches used in the topology reported in Fig. 3(b)

Reference	Part Number	Q_g ($V_d = 6V$)	R_{dsON}	C_{oss}
Q_1-Q_4	BSZ025N04LS	23nC	2.5m Ω	750pF
Q_5-Q_{10}	BSZ013NE2LS5I	25nC	1.3m Ω	1200pF

TABLE III: Total MOSFET loss comparison at different switching frequencies with $V_{IN} = 54V$, $I_{OUT} = 50A$.

f_{sw}	P_{dr}	P_{MOSsw}	$P_{MOScond}$ at $I_{OUT} = 25A$	$P_{MOScond}$ at $I_{OUT} = 50A$
200kHz	290mW	175mW	1.78W	7.15W
400kHz	580mW	350mW	1.78W	7.15W
800kHz	1.16W	700mW	1.78W	7.15W

the minimum amount of capacitors is determined by their capability of supporting the max RMS current expressed in (12). Obviously better efficiency performance can be reached by increasing the capacitor values in order to reduce the total ESR. After defining the value of C_R , the value of L_R is determined by the operating frequency f_{sw} . The inductance is dimensioned considering the maximum peak current and the rms current, reported respectively in (11) and (12). The voltage stress of the switches has been already discussed in the previous session. The maximum current is expressed by (11) and the RMS current is $1/\sqrt{2}$ of the value calculated by (12). Finally each loss contribution can be calculated. The losses of the passive components in each building block can be calculated by I_{CRMSm} and the ac resistance. The loss related to each MOSFET has three main contributions: the conduction loss, the C_{oss} loss due to the ZCS working condition, and the gate driver loss. Considering each MOSFET conducts I_{CRMSm} for one half of the period T_{sw} and the drain source voltage during the dead time T_d before the next turn on approximatively equals to one half of V_{dsOFF} , each MOSFET loss can be expressed as below.

$$\begin{aligned} P_{MOS} &= P_{MOScond} + P_{MOSsw} + P_{dr} \\ &= R_{dsON} \frac{I_{CRMSm}^2}{2} \\ &\quad + \left(\frac{V_{dsOFF}}{2} \right)^2 C_{oss} f_{sw} + V_{dr} Q_g f_{sw} \end{aligned} \quad (13)$$

Even if P_{MOSsw} and P_{dr} create a frequency limitation, these two contributions aren't dominant for the STC architecture reported in Fig. 3-6, in which V_{dsOFF} is V_{out} or $2V_{out}$. In fact considering the 4-to-1 STC topology reported in Fig. 3(b) with an input voltage $V_{IN} = 54V$, a maximum output current of $I_{OUT} = 50A$ and the switches listed in Table II, the total MOSFET losses (reported in Table III for different switching frequencies) are modest compared with the output power ($P_{out} \cong 650W$ at maximum load).

V. IMMUNITY TO COMPONENT MISMATCHES

Most of STCs topologies contain more than one resonant tank with mutual mismatches. Considering the 4-to-1 topology

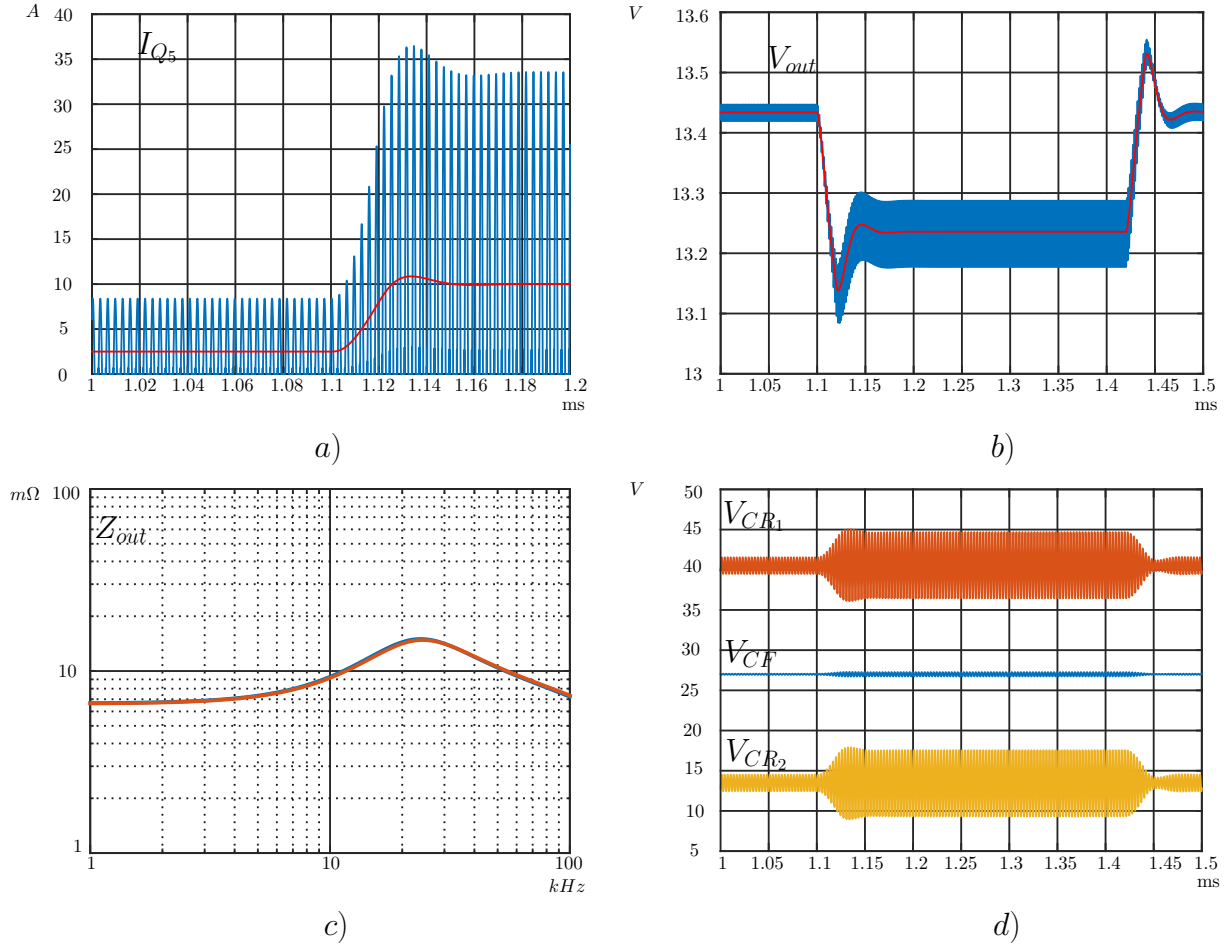


Fig. 10: Transient waveform comparisons of the converter of Fig. 3(b) and its SSA model of Fig. 9 during a load transient from 10A to 40A: (a) I_{Q_5} outgoing current taken as positive of Fig. 3(b) (blue line) and I_{Leq1} of Fig. 9 (red line); (b) Output voltage V_{out} of Fig. 3(b) (blue line) and of the SSA model (red line); (c) Simulation of the output impedance of the converter (blue line) and of the model (red line). In (d) is reported the voltage ripple of V_{CR_1} , V_{CR_2} and V_{CF} during the load transient.

reported in Fig. 3(b) with a small dead time T_d , the effect of the mismatch on the resonant tanks (worst case with $L_R \pm 10\%$ and $C_R \pm 5\%$) is reported in Fig. 11(a). The resonant tank with shortest T_R exhibits a bigger RMS current and the ZCS conditions are lost for both turn-on and turn-off of the switches. A higher dead time T_d reduces difference in the RMS current as can be seen in Fig. 11(b) but the switch turn-off conditions are not optimal and body diode conduction losses are present. The best solution is based on managing the ON time of each individual switch in order to achieve the ZCS during the switching transition. This operation can be obtained by using some zero crossing detection techniques in the controller or drivers to trigger the turn-off of the devices. Obviously the dead time T_d reported in the Fig. 8 must be sufficiently large to compensate the maximum mismatch between different resonant periods T_{Ri} . In other words in a topology with N_R resonant building blocks the T_{sw} is larger than the maximum T_{Ri} as reported in the next equation.

$$T_{sw} > \max_{1 \leq i \leq N_R} T_{Ri} \quad (14)$$

The impact of the mismatches on the current sharing can be

easily predicted by the SSA model reported in the previous section. Each resonant building block impedance Z_{eqi} can be calculated by using a different resonant period T_{Ri} in the equations (7) and (8). The non-resonant building blocks are conducting resonant current with two different T_{Ri} in the two switching states. The equivalent resistance can be calculated by using (8) and considering the mean value of the two T_{Ri} . STC topologies such as Fig. 3, Fig. 4 and Fig. 5 have a balanced current among the building blocks even if their impedances are mismatched. This consideration can be easily verified by the series connection of the equivalent DCX blocks reported in Fig. 9. For STC parallel operations, the current sharing accuracy within the two phases shown in Fig. 6 depends on the worst case mismatch of the two equivalent output resistances R_{eqout} of each phase calculated by (9). The variation of the phase output current I_{out} is simply derived and reported in the equation below.

$$\left| \frac{\Delta I_{out}}{I_{out}} \right| = \left| \frac{\Delta R_{eqout}}{R_{eqout}} \right| \quad (15)$$

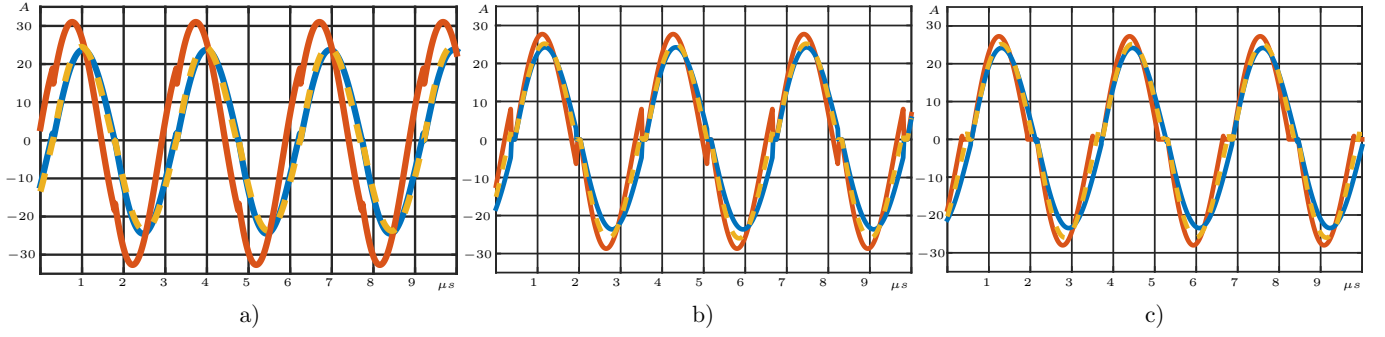


Fig. 11: Effect of the resonant tank mismatches (worst case with $L_R \pm 10\%$ and $C_R \pm 5\%$) on the two inductor currents I_{LR} (red and blue lines) of the converter reported in Fig. 3(b) at 30A compared with nominal condition (dashed yellow line): (a) solution with T_d of 10nsec; (b) solution with T_d of 100nsec; (c) using adaptive ON time control.

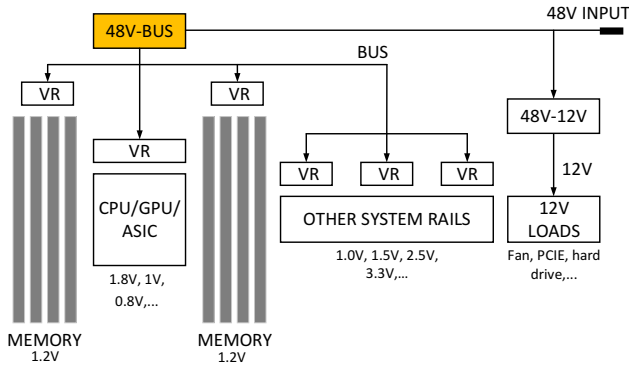


Fig. 12: Proposed power system architecture for 48V data center server board.

VI. STC APPLICATION IN DATA CENTER

Benefiting from all the unique electrical characteristics discussed above, the proposed STC topologies can extraordinarily address the SCC technical challenges described in Section II. This makes the adoption of STCs for industry's mass production design much easier. The proposed STCs are widely applicable to high ratio DC-DC bus conversions where galvanic isolation is not a requirement. 48V data center power system is one of the emerging applications that can very well leverage the advantages of STC. Fig. 12 shows the proposed power system architecture for a typical 48V server board in data center. A two-stage conversion approach is adopted here for the micro-processor (CPU, GPU, ASIC, etc.) core rails, memory rails and other system house-keeping rails. The first stage bus converter uses an STC to step down the input 48V bus to an intermediate voltage bus. Single-phase or multi-phase buck regulators are used for the second stage point-of-load power conversions. The voltage of the intermediate bus can be optimally selected to achieve the best overall performance in terms of efficiency, density and cost. Fig. 13 shows a 4-to-1 STC bus converter architecture implemented with the control and driving system. As reported in the schematic the controller generates two pairs of complementary gate driver signals $G_1\phi$, $G_1\bar{\phi}$ and $G_2\phi$, $G_2\bar{\phi}$ with different dead time T_d . The correct dead time T_d in order to achieve ZCS operation for each resonant tank is obtained by monitoring the switching

TABLE IV: Key parameters and components of the 4-to-1 STC in Fig. 13

Input voltage V_{in}	40V-60V, 54V nominal
Output voltage V_{out}	9.5V-15V, 13.5V nominal
Output current I_{out}	50A
C_R	3.8uF (0.47uF, 50V, U2J, +/-5%, 8pcs, Kemet)
L_R	58nH (PA5013, +/-4nH, Pulse)
C_F	60uF (10uF, 50V, X7R, 12pcs, Murata)
C_{IN}	35uF (10uF, 100V, X7S, 12pcs, Murata)
C_{OUT}	470uF polymer + 140uF MLCCs
$Q_1 - Q_4$	BSZ025N04LS (40V, 2.5mOhm)
$Q_5 - Q_{10}$	BSZ013NE2LS5I (25V, 1.3mOhm)
F_{sw}	320kHz
STC controller	STNRG328A (STMicro)
Gate driver	STRG04 (STMicro)
Buck controller	LTC7801 (Linear Tech)

node V_{1s} for the first tank and V_{2s} for the second tank. Zero current detection for each tank can be obtained by checking the body diode conduction state of Q_5 , Q_6 , Q_9 and Q_{10} during T_d or by measuring the on-state voltage drop of each FET. A simple and scalable charge pump circuit is designed to generate bias power for each gate driver. A front-end buck converter is incorporated for STC start-up and protections. Upon start up, the STC controller generates PWM signals first to the STC power train and then enables the buck converter to ramp up. At steady state, the buck converter operates with 100% duty cycle to offer a 99.9% efficiency. Meanwhile, the buck inductor serves as the input filter for STC. When the STC controller detects a fault event, it immediately shuts down the buck converter such that every voltage in the downstream of the buck can be safely discharged. Detailed circuit design and operations are not in the scope of this paper.

VII. EXPERIMENTAL RESULTS

A 650W 4-to-1 STC product evaluation board shown in Fig. 14 has been designed for the data center 48V bus conversion. The key parameters and components are listed in Table IV. To avoid confusion, the 48V bus specifications here are based on Google data center power rack. As seen in Fig. 14, even though components are loosely populated to meet Google's data center

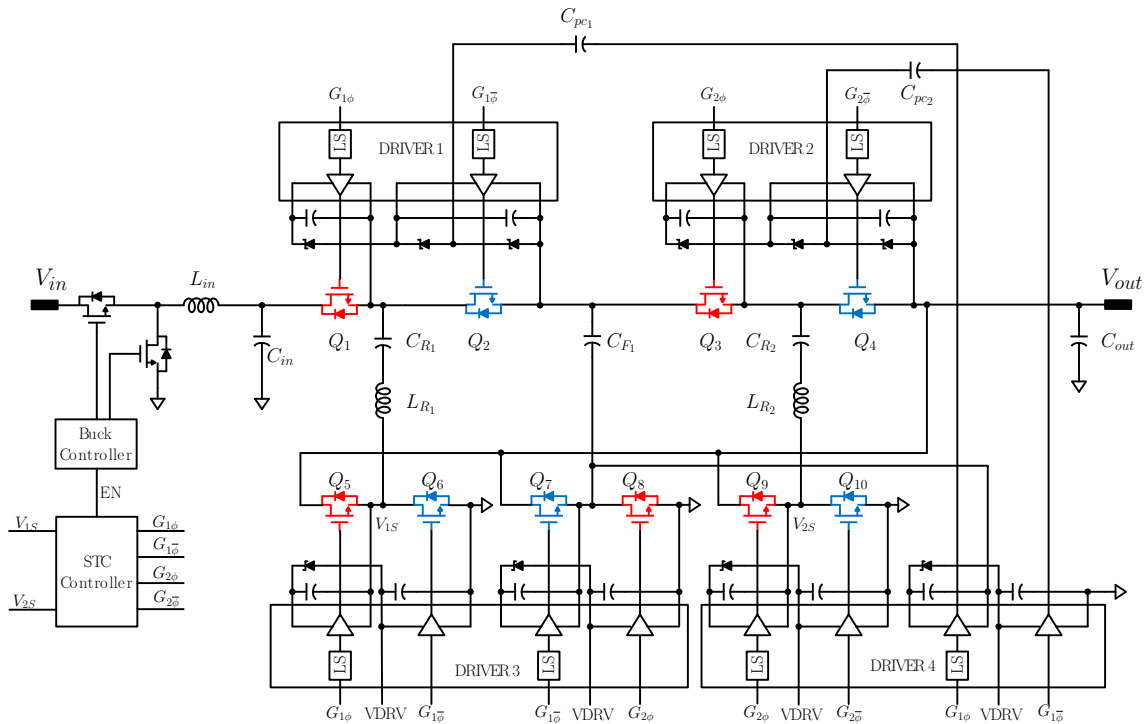
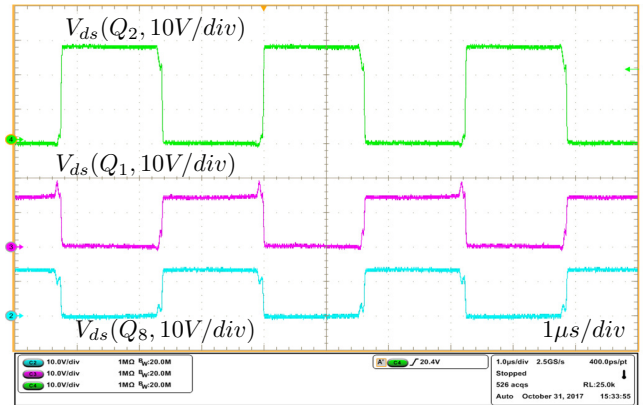
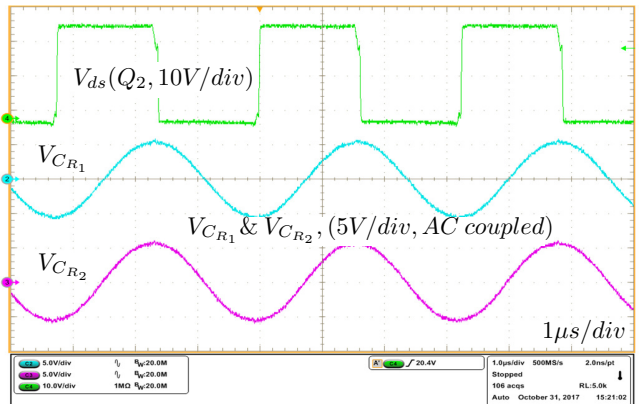


Fig. 13: STC architecture with the control and driving system.

DFM requirements, a very high power density of 500W/inch² is achieved with the STC power train. The driver and control circuitries can be potentially integrated by semiconductor manufacturers to offer an overall compact solution. As can be seen in Table IV, L_R is a high current shielded inductor with low emission [40] and low tolerance, C_R is composed by Class I (U2J) capacitors and T_{sw} corresponds to the relation (14).



a)



b)

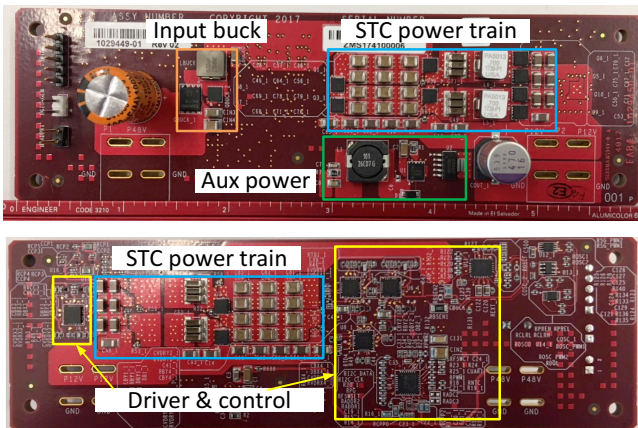
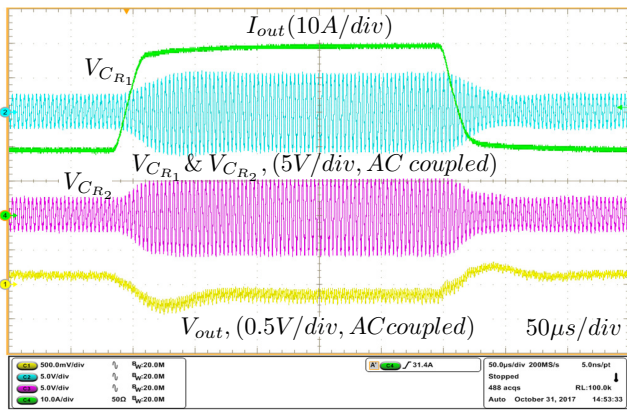
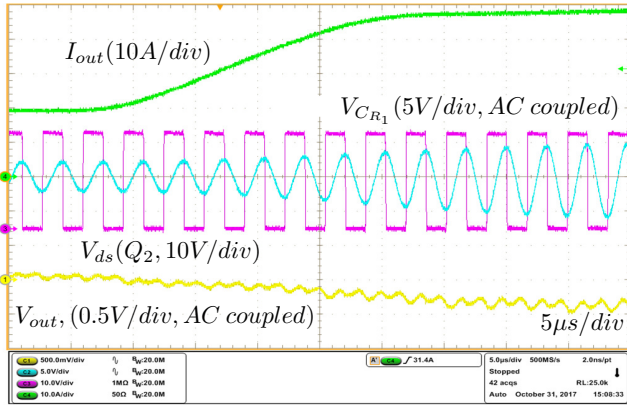


Fig. 14: 650W 4-to-1 STC product evaluation board.

Fig. 15: STC Steady state waveforms ($V_{in}=54V$, $I_{out}=50A$):(a) V_{ds} voltages of Q_1 , Q_2 and Q_8 ,(b) Voltage across the capacitors $C_{R1,2}$.



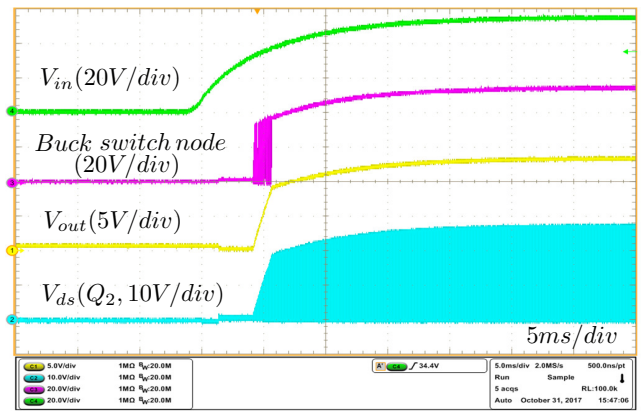
a)



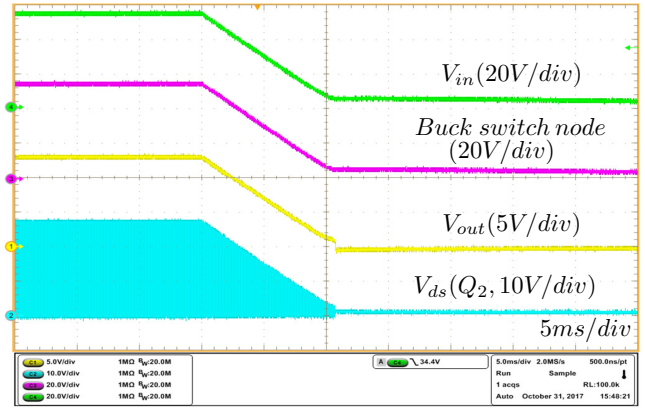
b)

Fig. 16: STC load transient waveforms ($V_{in}=54V$, $I_{out}=20A-50A$):(a) V_{out} , $V_{C_{R1,2}}$ and I_{out} ,(b) detail of load step up transient with V_{ds} voltages of Q_2 .

Fig. 15(a) shows the steady state waveforms of the drain-to-source voltages across Q_1 , Q_2 and Q_8 . In this 4-to-1 STC, the maximum voltage stress for Q_1-Q_4 is $2V_{out}$. However, for Q_1 and Q_4 , the nominal blocking voltage is V_{out} ; during the dead time (100ns in this design), the voltage stress may increase up to $2V_{out}$ due to switching timing mismatches. All the output SR FETs (Q_5-Q_{10}) have the maximum voltage stress of V_{out} . Benefiting from zero current switching, switching spikes can barely be seen with each FET. In Fig. 15(b), the sine-wave voltage ripples across capacitor C_{R1} and C_{R2} are shown. The peak and valley are both aligned with the switching edges to achieve ZCS. Due to the charge balance principle, the currents in both resonant tanks are automatically balanced. Shown on Fig. 16 are the waveforms during the load step transients. The STC demonstrates an intrinsically fast response as there are very little energy storage components in the topology. Fig. 17 shows the start up and shut down waveforms of STC. Upon start up, the bias power becomes available first when V_{in} reaches around 15V. At the same time, the STC controller generates switching signals to the STC power train. After a short delay (3ms), the STC controller issues an enable signal to the input buck for ramp up. The buck converter eventually enters bypass mode (100% duty cycle) once its output voltage reaches the input.



a)



b)

Fig. 17: STC startup (a) and shut down (b) transient main waveforms: V_{in} , Buck switch node, V_{out} and V_{ds} voltages of Q_2 .

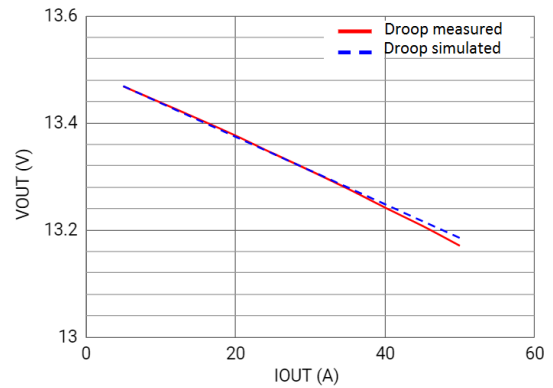
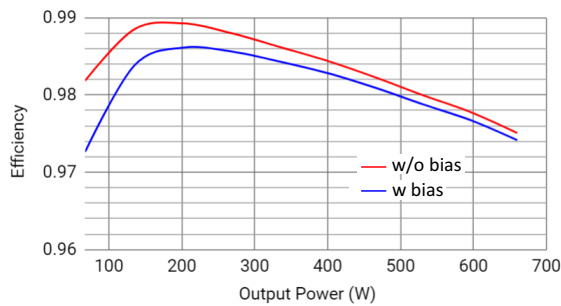


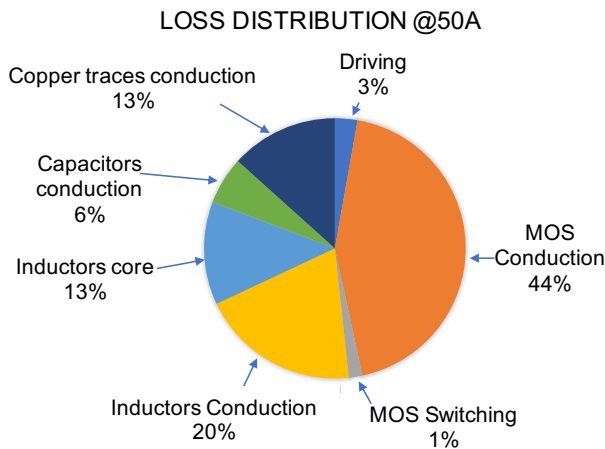
Fig. 18: STC output voltage v.s. output current ($V_{in}=54V$) (red line) and the simulated value by using the model (dashed blue line).

The STC output voltage droop characteristics has been measured and shown in Fig. 18. It verifies the STC output resistance model predicted by (9). And this droop characteristic allows multiple STCs for parallel operation when their internal AC resistances are well matched. Fig. 19(a) demonstrates the

superior efficiency performance of the STC topology. The 4-to-1 STC evaluation board achieves a very high peak efficiency of 98.92% excluding bias power and 98.61% with bias power. At full load, 97.51% without bias and 97.41% with bias are still maintained. In Fig. 19(b) the loss breakdown at full load is reported. It is shown that the total loss is dominated by the conduction loss in the switches and the passive components. Optimizing the core-winding structure and taking better care of winding ACRs may further improve the full load efficiency. Fig. 20 shows the thermal image of the STC board with fan cooling only at full load and room temperature. It shows an extraordinary thermal performance without any heat sink, which significantly simplifies the thermal management in data center server board designs. This STC design can be easily scaled for higher power specifications by using off-the-shelf standardized components only. In Fig. 21 is reported a 1.2kW STC design with the thermal performance under fan cooling at full load. Finally in Fig. 22 is reported a mass-production 48V server system design that employs a 4-to-1 STC as the first bus voltage conversion stage.

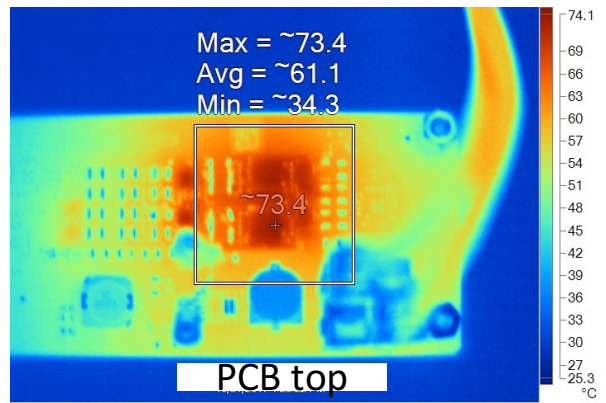


a)

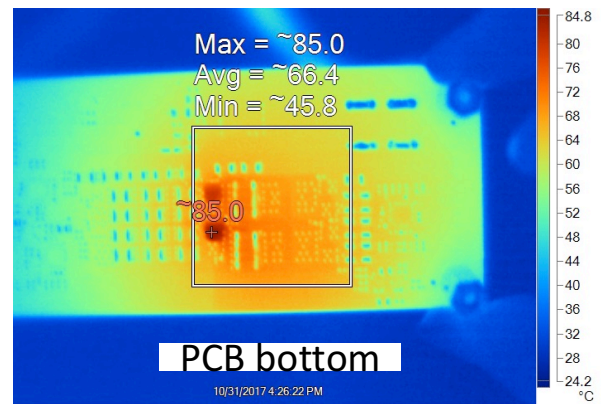


b)

Fig. 19: (a) STC efficiency with and without bias power ($V_{in}=54V$); (b) loss breakdown at full load.



a)



b)

Fig. 20: STC thermal performance with fan cooling only ($V_{in}=54V$, $I_{out}=50A$, $T_a=25^\circ C$).

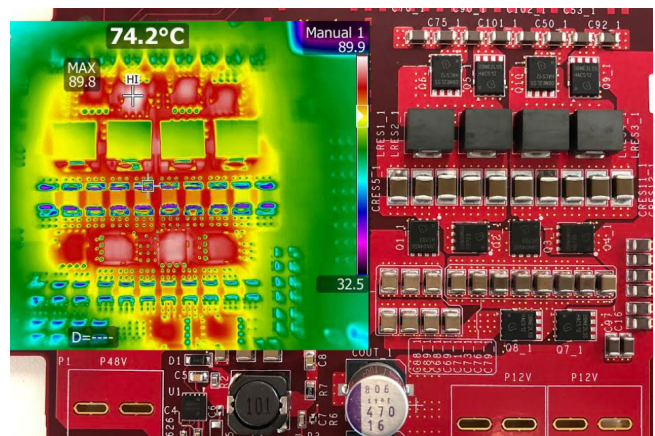


Fig. 21: STC 1.2KW design, thermal performance with fan cooling ($V_{in}=54V$, $I_{out}=92A$, $T_a=25^\circ C$).

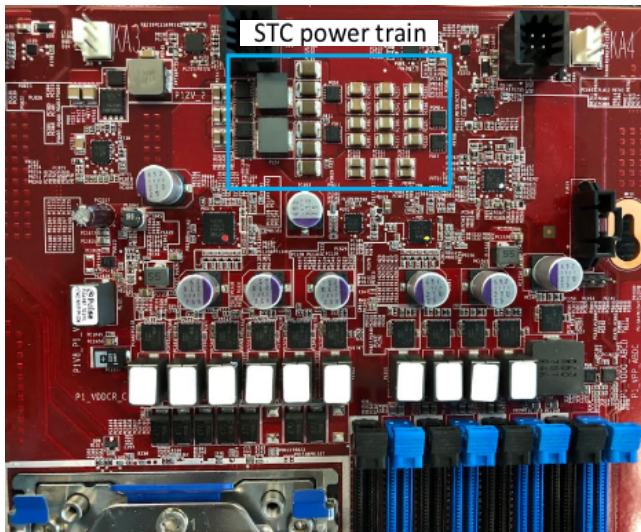


Fig. 22: A mass-production 48V server that incorporates STC for first stage bus conversion.

VIII. CONCLUSION

This paper has presented a new class of Switched Tank Converters for very high efficiency high density DC-DC power conversion where high conversion ratio is required. The STCs uniquely employ LC resonant tanks to partially replace the DC flying capacitors in traditional switched capacitor converters, thus providing complete soft charging, soft switching and minimal device voltage stresses under all operating conditions. The proposed STC topologies overcome the fundamental technical barriers of existing SCC derivative topologies by offering strong robustness against component non-idealities, control simplicity, and extraordinary scalability. Therefore, all these features of STCs have expedited the technology maturity for industry's high volume adoption. In addition to the proposal of the STC topology, an equivalent DCX building block principle has been introduced as a simple and effective analytical tool to better understand the STCs. The same principle can also be applied to analyze other SCC based topologies or derive new topologies. This paper focuses on one of the emerging applications, 48V data center server board power delivery. A 650W 4-to-1 STC evaluation board was designed for the 48V bus converter. Experimental results have been presented to demonstrate the STC operation principles, electrical characteristics, and superior performance (efficiency, density, thermal, etc.). It should be noted that STCs can be applied to a very broad range of power conversion. Due to the scope limit, many implementation details such as gate driver design, fault protections, input buck design, component integrations, layout considerations, adaptive PWM control schemes and so on are not discussed in this paper.

REFERENCES

- [1] X. Li and S. Jiang, "Google 48V power architecture," 2017 IEEE Applied Power Electronics Conference and Exposition (APEC), Tampa, FL, 2017, Keynotes presentation.
- [2] J. S. Brugler, "Theoretical performance of voltage multiplier circuits," in IEEE Journal of Solid-State Circuits, vol. 6, no. 3, pp. 132-135, June 1971.
- [3] J. F. Dickson, "On-chip high-voltage generation in MNOS integrated circuits using an improved voltage multiplier technique," in IEEE Journal of Solid-State Circuits, vol. 11, no. 3, pp. 374-378, June 1976.
- [4] F. Ueno, T. Inoue, I. Oota and I. Harada, "Emergency power supply for small computer systems," 1991., IEEE International Symposium on Circuits and Systems, 1991, pp. 1065-1068 vol.2.
- [5] K. D. T. Ngo and R. Webster, "Steady-state analysis and design of a switched-capacitor DC-DC converter," in IEEE Transactions on Aerospace and Electronic Systems, vol. 30, no. 1, pp. 92-101, Jan 1994.
- [6] S. V. Cheong, H. Chung and A. Ioinovici, "Inductorless DC-to-DC converter with high power density," in IEEE Transactions on Industrial Electronics, vol. 41, no. 2, pp. 208-215, Apr 1994.
- [7] M. S. Makowski and D. Maksimovic, "Performance limits of switched-capacitor DC-DC converters," Power Electronics Specialists Conference, 1995. PESC '95 Record., 26th Annual IEEE, Atlanta, GA, 1995, pp. 1215-1221 vol.2.
- [8] M. Xu, J. Sun and F. C. Lee, "Voltage divider and its application in the two-stage power architecture," Twenty-First Annual IEEE Applied Power Electronics Conference and Exposition, 2006. APEC '06., Dallas, TX, 2006.
- [9] Y. K. Ramadass and A. P. Chandrakasan, "Voltage Scalable Switched Capacitor DC-DC Converter for Ultra-Low-Power On-Chip Applications," 2007 IEEE Power Electronics Specialists Conference, Orlando, FL, 2007, pp. 2353-2359.
- [10] M. D. Seeman and S. R. Sanders, "Analysis and Optimization of Switched-Capacitor DCDC Converters," in IEEE Transactions on Power Electronics, vol. 23, no. 2, pp. 841-851, March 2008.
- [11] V. W. Ng and S. R. Sanders, "A High-Efficiency Wide-Input-Voltage Range Switched Capacitor Point-of-Load DCDC Converter," in IEEE Transactions on Power Electronics, vol. 28, no. 9, pp. 4335-4341, Sept. 2013.
- [12] M. Chen, K. K. Afridi and D. J. Perreault, "Stacked Switched Capacitor Energy Buffer Architecture," in IEEE Transactions on Power Electronics, vol. 28, no. 11, pp. 5183-5195, Nov. 2013.
- [13] F. Z. Peng, F. Zhang and Z. Qian, "A magnetic-less DC-DC converter for dual-voltage automotive systems," in IEEE Transactions on Industry Applications, vol. 39, no. 2, pp. 511-518, Mar/Apr 2003.
- [14] F. H. Khan and L. M. Tolbert, "A Multilevel Modular Capacitor-Clamped DCDC Converter," in IEEE Transactions on Industry Applications, vol. 43, no. 6, pp. 1628-1638, Nov.-dec. 2007.
- [15] S. R. Sanders, E. Alon, H. P. Le, M. D. Seeman, M. John and V. W. Ng, "The Road to Fully Integrated DCDC Conversion via the Switched-Capacitor Approach," in IEEE Transactions on Power Electronics, vol. 28, no. 9, pp. 4146-4155, Sept. 2013.
- [16] C. K. Tse, S. C. Wong and M. H. L. Chow, "On lossless switched-capacitor power converters," in IEEE Transactions on Power Electronics, vol. 10, no. 3, pp. 286-291, May 1995.
- [17] Michael Evzelman, Shmuel Ben-Yaakov, "Average-Current-Based Conduction Losses Model of Switched Capacitor Converters," in IEEE Transactions on Power Electronics, vol. 28, no. 7, pp. 3341 - 3352, July. 2013.
- [18] R. C. N. Pilawa-Podgurski, D. M. Giuliano and D. J. Perreault, "Merged two-stage power converter architecture with soft charging switched-capacitor energy transfer," 2008 IEEE Power Electronics Specialists Conference, Rhodes, 2008, pp. 4008-4015.
- [19] D. M. Giuliano, M. E. DAsaro, J. Zwart and D. J. Perreault, "Miniaturized Low-Voltage Power Converters With Fast Dynamic Response," in IEEE Journal of Emerging and Selected Topics in Power Electronics, vol. 2, no. 3, pp. 395-405, Sept. 2014.
- [20] V. Yousefzadeh, E. Alarcon and D. Maksimovic, "Three-level buck converter for envelope tracking applications," in IEEE Transactions on Power Electronics, vol. 21, no. 2, pp. 549-552, March 2006.
- [21] D. Cao and F. Z. Peng, "Zero-Current-Switching Multilevel Modular Switched-Capacitor DCDC Converter," in IEEE Transactions on Industry Applications, vol. 46, no. 6, pp. 2536-2544, Nov.-Dec. 2010.
- [22] Y. Lei and R. C. N. Pilawa-Podgurski, "A General Method for Analyzing Resonant and Soft-Charging Operation of Switched-Capacitor Converters," in IEEE Transactions on Power Electronics, vol. 30, no. 10, pp. 5650-5664, Oct. 2015.
- [23] P. S. Shenoy, M. Amaro, J. Morroni and D. Freeman, "Comparison of a Buck Converter and a Series Capacitor Buck Converter for High-Frequency, High-Conversion-Ratio Voltage Regulators," in IEEE Transactions on Power Electronics, vol. 31, no. 10, pp. 7006-7015, Oct. 2016.
- [24] O. Keiser, P. K. Steimer and J. W. Kolar, "High power resonant Switched-Capacitor step-down converter," 2008 IEEE Power Electronics Specialists Conference, Rhodes, 2008, pp. 2772-2777.

- [25] D. Cao, X. Lyu and Y. Li, "Multilevel modular converter with reduced device count for hybrid and electric vehicle," 2015 IEEE Transportation Electrification Conference and Expo (ITEC), Dearborn, MI, 2015, pp. 1-6.
- [26] K. K. Law, K. W. E. Cheng and Y. P. B. Yeung, "Design and analysis of switched-capacitor-based step-up resonant converters," in IEEE Transactions on Circuits and Systems I: Regular Papers, vol. 52, no. 5, pp. 943-948, May 2005.
- [27] K. Kesarwani, R. Sangwan and J. T. Stauth, "Resonant-Switched Capacitor Converters for Chip-Scale Power Delivery: Design and Implementation," in IEEE Transactions on Power Electronics, vol. 30, no. 12, pp. 6966-6977, Dec. 2015.
- [28] Y. Lei, R. May and R. Pilawa-Podgurski, "Split-Phase Control: Achieving Complete Soft-Charging Operation of a Dickson Switched-Capacitor Converter," in IEEE Transactions on Power Electronics, vol. 31, no. 1, pp. 770-782, Jan. 2016.
- [29] Y. Li, B. Curuvija, X. Lyu and D. Cao, "Multilevel Modular Switched-Capacitor Converter with Voltage Regulation," 2017 IEEE Applied Power Electronics Conference and Exposition (APEC), Tampa, FL, 2017, pp. 88-93.
- [30] K. Zou, M. J. Scott and J. Wang, "A Switched-Capacitor Voltage Tripler With Automatic Interleaving Capability," in IEEE Transactions on Power Electronics, vol. 27, no. 6, pp. 2857-2868, June 2012.
- [31] K. Sano and H. Fujita, "Performance of a High-Efficiency Switched-Capacitor-Based Resonant Converter With Phase-Shift Control," in IEEE Transactions on Power Electronics, vol. 26, no. 2, pp. 344-354, Feb. 2011.
- [32] M. Shen, "A zero voltage switching switched capacitor voltage doubler," 2012 IEEE International Symposium on Industrial Electronics, Hangzhou, 2012, pp. 131-136.
- [33] D. Cao, X. Lu, X. Yu and F. Z. Peng, "Zero voltage switching double-wing multilevel modular switched-capacitor DC-DC converter with voltage regulation," 2013 Twenty-Eighth Annual IEEE Applied Power Electronics Conference and Exposition (APEC), Long Beach, CA, 2013, pp. 2029-2036.
- [34] Y. Li, J. Chen, M. John, R. Liou and S. R. Sanders, "Resonant switched capacitor stacked topology enabling high DC-DC voltage conversion ratios and efficient wide range regulation," 2016 IEEE Energy Conversion Congress and Exposition (ECCE), Milwaukee, WI, 2016, pp. 1-7.
- [35] Y. P. B. Yeung, K. W. E. Cheng, S. L. Ho, K. K. Law and D. Sutanto, "Unified analysis of switched-capacitor resonant converters," in IEEE Transactions on Industrial Electronics, vol. 51, no. 4, pp. 864-873, Aug. 2004.
- [36] J. T. Stauth, M. D. Seeman and K. Kesarwani, "Resonant Switched-Capacitor Converters for Sub-module Distributed Photovoltaic Power Management," in IEEE Transactions on Power Electronics, vol. 28, no. 3, pp. 1189-1198, March 2013.
- [37] A. Stillwell and R. C. N. Pilawa-Podgurski, "A resonant switched-capacitor converter with GaN transistors for series-stacked processors with 99.8% power delivery efficiency," 2015 IEEE Energy Conversion Congress and Exposition (ECCE), Montreal, QC, 2015, pp. 563-570.
- [38] A. Cervera, M. Evzelman, M. Peretz; S. Ben-Yaakov "A High-Efficiency Resonant Switched Capacitor Converter With Continuous Conversion Ratio," in IEEE Transactions on Power Electronics, vol. 30, no. 3, pp. 1373 - 1382, Apr. 2014.
- [39] A. Cervera, M. M. Peretz and S. Ben-Yaakov, "A Generic and Unified Global-Gyrator Model of Switched-Resonator Converters," in IEEE Transactions on Power Electronics, vol. 32, no. 12, pp. 8945-8952, Dec. 2017.
- [40] F H Alexander Gerfer "7 Design tips for selection of power inductors" 2016 IEEE 2nd Annual Southern Power Electronics Conference (SPEC), 2016, pp. 1-4.
- [41] S. Ben-Yaakov, "Behavioral average modeling and equivalent circuit simulation of switched capacitors converters" IEEE Trans. on Power Electronics , 27, 2, 632-636, 2012.
- [42] S. Ben-Yaakov, "On the influence of switch resistances on switched-capacitor converter losses" IEEE Trans. on Industrial Electronics, Letters, 59, 1, 638-640, 2012.
- [43] M. Evzelman, S. Ben-Yaakov, "Simulation of hybrid converters by average models." IEEE Transactions on Industry Applications, 50, 2, 1106-1113, 2014.